

Droplet Microreactors

Controlled Crystallization of Sodium Chloride Nanocrystals in Microdroplets Produced by Electrospray from an Ultra-Dilute Solution

Fuqin Zheng,^[a] Dong Wang,^[c] Hairui Fang,^[b] Haidong Wang,^[a] Meng Wang,^[b] Keke Huang,^[b] Huanwen Chen,^{*[a,b]} and Shouhua Feng^{*[b]}

Abstract: Controlled crystallization is very important for crystal growth. The electrospray (ES) technique has attracted great interest thanks to its advantages of facile manipulation of micrometer droplets and the generation of fine and charged droplets with very narrow size dispersion. In this work, nanocrystals with cubic shapes with 32 nm edges were successfully grown from ultra-dilute NaCl solution (1 $\mu\text{g mL}^{-1}$) on a millisecond timescale by an ES technique. Dispersed and charged microdroplets were created by ES. In the process, an increase in ion strength and built-in electric field in microdroplets promoted nucleation and

growth. Moreover, solvent evaporation increased solute and charge concentration and decreased the size of the microdroplets, which had a further effect on nucleation and growth. The morphologies of crystals were the competitive results of ion strength and evaporation. Fortunately, these physicochemical properties can be controlled facilely by adjusting the ES parameters. This report suggests potential application of ES technology for controllable crystallization of pharmaceuticals, proteins, etc.

Introduction

Understanding the process of crystallization is of great importance for designed synthesis and the preparation of crystalline materials.^[1,2] However, crystallization processes in general are probabilistic and poorly developed, especially the formation of nuclei that eventually leads to crystal growth.^[3] For the past few years, microfluidic technology has been attracting great interest due to its potential for precise manipulation of small quantities of fluids constrained in channels of dimensions from micrometers to millimeters.^[4,5] In addition, localization and in situ characterization may be carried out during the experiment by spectroscopic techniques^[6] or diffraction^[7,8] studies. Zhu^[9] obtained LaF₃ nanoparticles with a mean diameter of 4.5 nm and LaPO₄ nanorods with lengths of 60–70 nm and diameters of 10–15 nm in a microfluidic reactor by microwave irradiation. Iyer^[10] synthesized CePO₄ nanorods decorated with emission-tunable quantum dots with excellent fluorescence properties. This technology is now widely used in various fields.

Electrospray (ES) techniques, also named electrohydrodynamic atomization (EHDA), are mainly applied in the ion sources of mass spectrometers.^[11–15] This technique has been attracting lots of attention for producing micro- and nanostructured materials since the 1990s.^[16] ES, in contrast with microfluidic methods, not only possesses those methods' advantages, but also has excellent characteristics such as generating fine, charged and narrow-sized droplets under the influence of electrical potential.^[17,18] Moreover, the concentration, droplet size, and ion strength of microdroplets will change rapidly under the conditions of solvent evaporation and high voltage, which have strong impacts on crystallization. Owing to the simplicity and flexibility of the ES experimental setup and the controllable polarity, charge and droplet size by adjusting the ES parameters, this technique has been successfully employed to generate particulate materials with controllable compositions, structures, sizes, morphologies, and shapes. It proved to be a continuous, simple, green, and effective method for nanocrystal growth.^[19–23] For example, Radacsi^[22] prepared nano-sized crystals of the pharmaceutical niflumic acid with dimensions of 200–800 nm. Lenggoro^[23] produced ZnS nanoparticles of 20–40 nm in size through systematic control of the key variables in electrospray pyrolysis. In addition, crystallization can occur in electrosprayed droplets on millisecond timescales. Moreover, Cooks prepared metallic nanobrushes by exploitation of the Coulombic forces present in the electrolytic spray system; this is expected to generate interest in this method for creating metallic crystals, thanks to its ease in fabricating such structures directly from solutions and the efficient control of size and composition.^[24] Therefore, ES technology has the potential to grow

[a] Jiangxi Key Laboratory for Mass Spectrometry and Instrumentation, East China University of Technology, Nanchang 330013, P. R. China
E-mail: chw8868@gmail.com
<http://www.sinoms.net/>

[b] State Key Laboratory of Inorganic Synthesis and Preparative Chemistry, Department College of Chemistry, Jilin University, Changchun 130012, P. R. China
E-mail: shfeng@mail.jlu.edu.cn

[c] Department of Chemical Engineering, Northeast Dianli University, Jilin City 132012, P. R. China

ORCID(s) from the author(s) for this article is/are available on the WWW under <http://dx.doi.org/10.1002/ejic.201501453>.

to become one of the future mainstream technologies for controlled preparation of crystals.

Sodium chloride, one of the simplest crystal systems, often serves as a test sample to explore the performance of crystal technology.^[25–27] For example, Z. Wang^[25] studied the influence of solution drying rate on crystallization of sodium chloride nanoparticles with various morphologies. T. Chen^[26] incorporated aerosol technology and a differential mobility analyzer to produce monodisperse NaCl nanoparticles with measured median diameter from 8.33 to 128 nm and geometric standard deviation from 1.04 to 1.08. However, there have been few investigations into using electrosprayed charged droplets to study the mutual influence of charge and evaporation on crystallization. In this study, charged droplets were prepared by ES with the simplest compound – sodium chloride – as test sample. The influence of ion strength and evaporation on crystallization from ultra-dilute NaCl solution ($1 \mu\text{g mL}^{-1}$) was investigated by adjusting parameters such as capillary voltage, solution flow rate, flight distance, and nebulizer gas flow rate.

Results and Discussion

Characterization of Crystals

The XRD pattern of an as-prepared sample is shown in Figure 1 (a). It was found that the NaCl crystal was well indexed in a cubic unit cell of space group $Fm\bar{3}m$ (ICDD-PDF 01-0994). The crystal orientation of the sample is marked at the positions corresponding to characteristic peaks. Other characteristic peaks marked with asterisks originate from the monocrystalline silicon substrate.

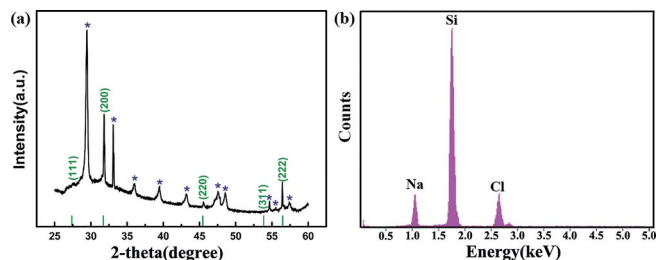


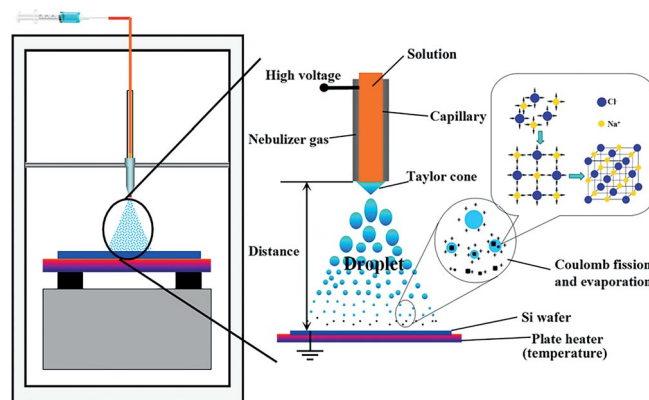
Figure 1. Structural analysis of crystals: (a) XRD, (b) EDX.

Energy-dispersive X-ray spectroscopy (EDX) results gave the elemental composition of the as-prepared sample. The EDX spectrum (see Figure 1, b) indicated the presence of Na, Cl, and Si (strong silicon signals were due to the silicon wafer used as deposition surface), but the absence of other elements, thus indicating that the NaCl crystal had a very high purity.

Formation of NaCl Nanocrystals

The dispersed and charged microdroplets were created by ES as shown in Scheme 1. In the process, the built-in electric field and the ion strength of the solvent in the microdroplets can affect the nucleation and growth of crystals.^[28] On the other hand, solvent evaporation from the microdroplets increased the ion concentration of the solution and decreased the sizes of

the droplets, and this had a further effect on nucleation and the growth of crystals.^[29] In addition, different evaporation rates in general resulted in various curves corresponding to increases in ion concentration and decreases in droplets size. As Z. Wang^[25] reported, the development of the morphology reflects the diffusive movement of NaCl monomers, and the diffusive movement of these monomers is facilitated by the water content of the particle. At one extreme of excessively rapid drying, water removal from the particle is faster than the movement of NaCl monomers, and then the crystallizing solute does not have enough time to form a euhedral crystal, corresponding to a morphology with rounded edges. In contrast, at the other extreme of excessively slow drying, there is sufficient time to form a crystal with a cube shape. Therefore, it is important to study the effect of ES parameters for crystallization. Below we give details of parameters used in the ES, the results of which are described in the subsequent sections.



Scheme 1. Illustration of setup for electrospray crystallization.

The Effects of Applied DC Capillary Voltage

The effects of applied capillary voltage on crystal nucleation and growth were investigated by ES with capillary voltage from 0 kV to +12 kV and at a substrate temperature of 150 °C. The morphologies and size distributions of the crystals are presented in Figure 2. It can be seen that the size distributions of the NaCl crystals fit the normal distribution and that the sizes of the crystals decreased with increasing capillary voltage. Without capillary voltage, the mean size of the crystals was 89 nm, ranging from 30 nm to 210 nm, with cubic, round, and irregular shapes. When the capillary voltage was increased to 12 kV, the mean size of the crystals decreased to 48 nm and size distribution became narrower, ranging from 68 to 20 nm and all with cubic shapes.

In our view, there are two effects on crystallization of NaCl nanocrystals with increasing voltage. Firstly, a higher voltage would help to overcome the surface tension of droplets and thus form smaller droplets with the continuous enhanced effect of evaporation and the Coulomb fission, which made it possible to produce aerosols with one charge and to form smaller droplets.^[30] Monodispersed and small crystals may thus be obtained. Secondly, the built-in electric field strength and ion

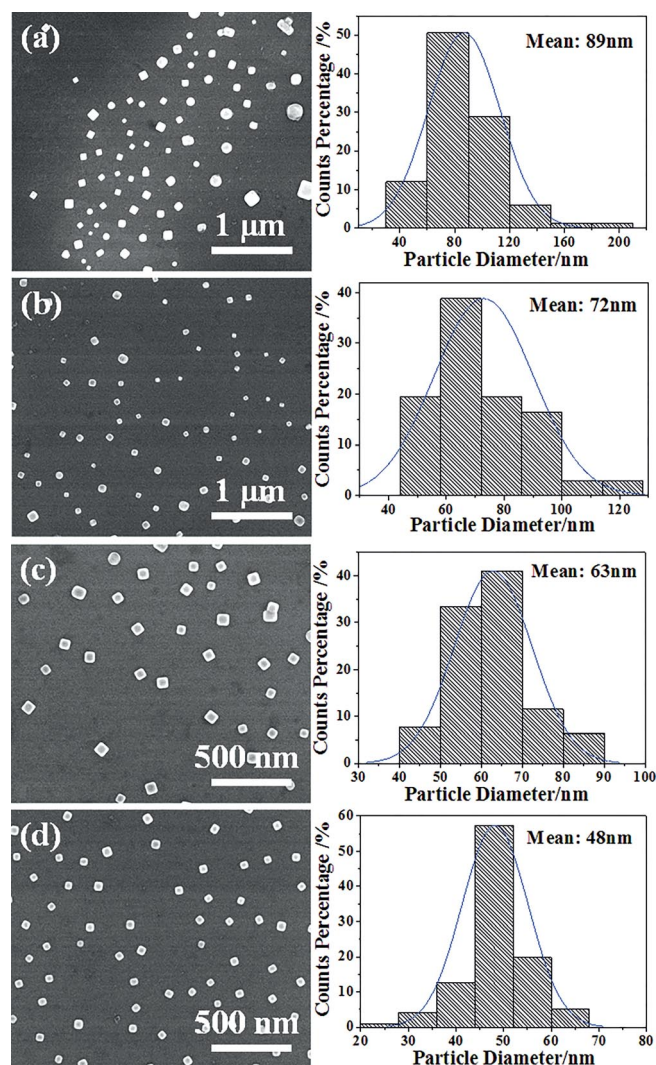


Figure 2. SEM images and nanocrystal size distributions at different capillary voltages: (a) 0 kV, (b) +4 kV, (c) +8 kV, (d) +12 kV. The sizes of crystals were measured with a Nano Measurer 1.2 instrument. Over 200 particles were measured for each sample.

strength increase in the charged microdroplets had a greater impact on crystal nucleation and growth.^[28] It demonstrated that an increase in the built-in electric field strength and ion strength was more favorable for making crystals smaller and more regular with cubic shapes, as shown by the SEM analysis in Figure 2.

The Effects of Liquid Flow Rate

SEM images and size distributions of the NaCl crystals at different liquid flow rates from 10 to 200 $\mu\text{L min}^{-1}$ and at a substrate temperature of 150 $^{\circ}\text{C}$ are shown in Figure 3. It can be seen that nanoparticles with larger sizes and wider size distributions were obtained at higher liquid flow rates. At a low liquid flow, regular nanocrystals with cubic shapes could be obtained. In contrast, at a high liquid flow, the nanocrystals tended to polydispersity.

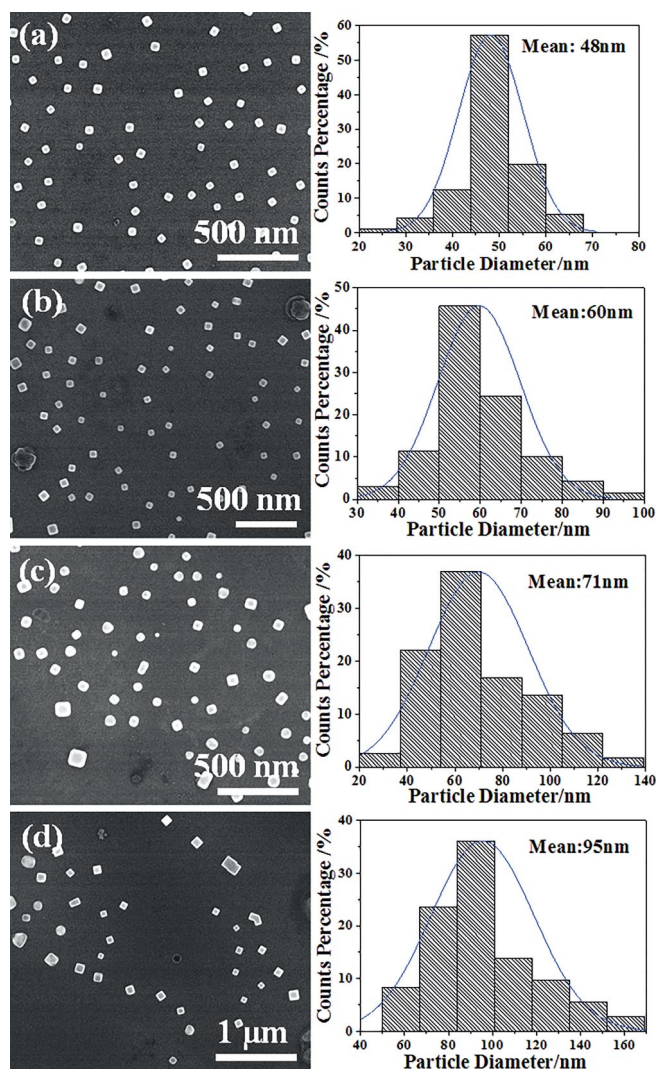


Figure 3. SEM images and nanocrystal size distributions at different solution flow rates: (a) 10 $\mu\text{L min}^{-1}$, (b) 50 $\mu\text{L min}^{-1}$, (c) 100 $\mu\text{L min}^{-1}$, (d) 200 $\mu\text{L min}^{-1}$.

Liquid flow rate is important for size distribution and for solvent evaporation from charged droplets. Gomez et al.^[31] and Ganan-Calvo et al.^[32] reported that a higher liquid flow rate always generated larger droplets with wider size distributions because it slowed down evaporation. Hence, larger droplets with lower solute concentrations, wider size distributions, and lower charge densities were obtained. The overall results, as revealed by SEM analysis, were an increase in crystal size, a broadening in size distribution, and a decrease in regularity. To obtain nano-sized crystals of smaller size, the liquid flow rate of 10 $\mu\text{L min}^{-1}$ was chosen as optimized parameter in the study because the mean size and distribution of crystals were at their minimum (see Figure 3, a).

The Effects of Flight Distance

SEM images and size distributions of NaCl crystals at different flight distances and at 150 $^{\circ}\text{C}$ are shown in Figure 4. It can be seen that increasing the flight distance led to a decrease in

the sizes of the NaCl crystals. We could obtain excellent cubic nanocrystals with a flight distance of 50 mm. However, when the flight distance was increased to 85 mm the nanocrystals became smaller but more dispersed in size.

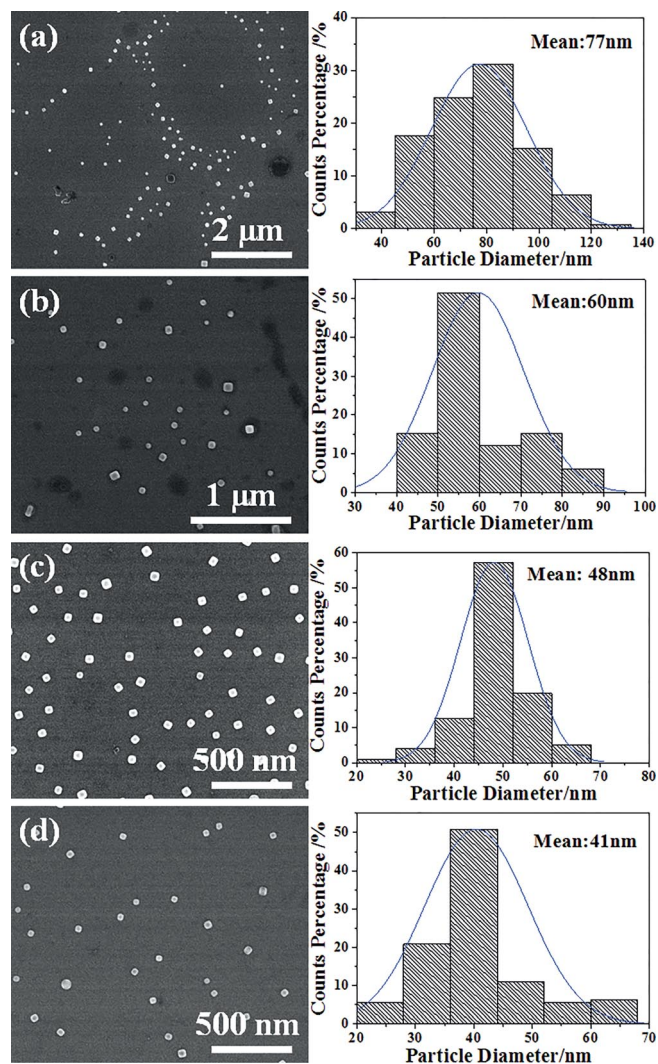


Figure 4. SEM images and nanocrystal size distributions at different distances from nozzle to the collector: (a) 20 mm, (b) 30 mm, (c) 50 mm, (d) 85 mm.

The temperature should decrease with the distance from the heater. In this study, the heater was fixed under the Si wafer. As the flight distance between the Si wafer and nozzle increased, the temperature of the nozzle decreased. In addition, the electro-spray droplets had a longer travel time. This meant that smaller droplets could be produced, due to more solvent evaporation and continuous effect of Coulomb fission, before deposition on the substrate.^[33,34] Thus, smaller, regular nanoparticles were more likely to be obtained. However, with increasing flight distance, the temperature near the nozzle was lower, leading to a longer time for crystal nucleation. This is not favorable for preparation of monodispersed nanoparticles. Therefore, the sizes of the crystals decreased, but the size distribution narrowed under 50 mm and broadened at 85 mm with the flight distance increasing, as shown in Figure 4.

The Effects of Nebulizer Gas Flow Rate

The influence of nebulizer gas flow rate on nucleation and growth of crystals at 150 °C is displayed in Figure 5. As can be seen, variation in the flow rate of liquid sample could give different results with regard to the morphologies and size distributions of the NaCl crystals. With increasing gas flow rate, the particle size was reduced to as low as 32 nm, but the crystal size distributions became broader when the gas flow rate was more than 80 mL min⁻¹. The gas flow rate of 60 mL min⁻¹ was chosen as an optimized condition for acquiring smaller and more regular cubic NaCl crystals.

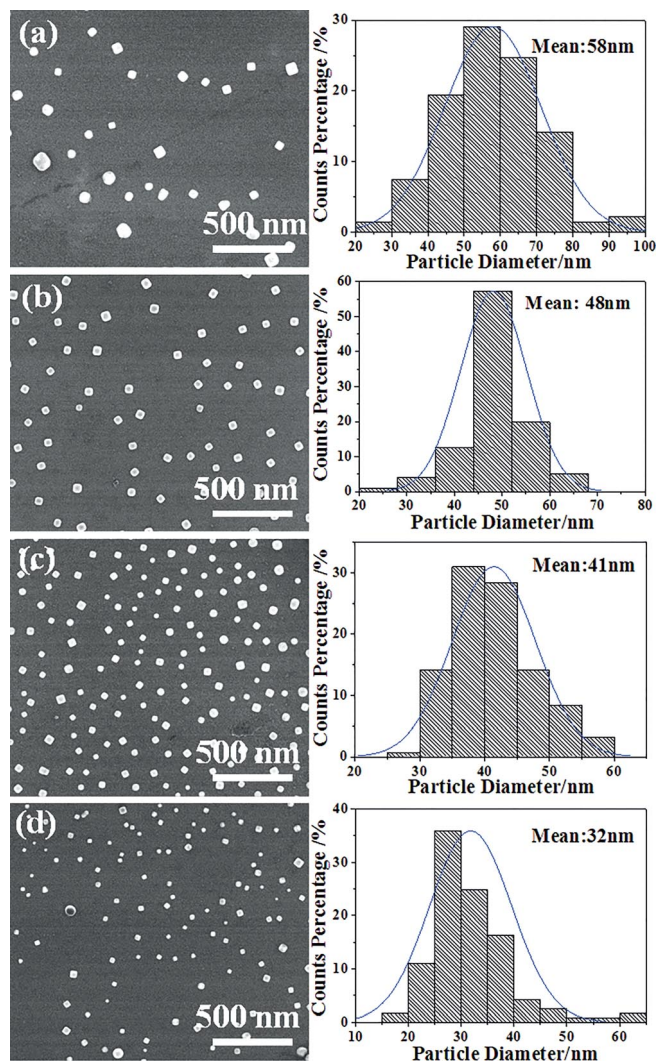


Figure 5. SEM images and nanocrystal size distributions at different nebulizer gas flow rates: (a) 40 mL min⁻¹, (b) 60 mL min⁻¹, (c) 80 mL min⁻¹, (d) 100 mL min⁻¹.

From theoretical analysis, the nebulizer gas can influence the electro-sprayed droplets during the spray process in three ways:^[35] (1) breakup of droplets, (2) acceleration of droplets, and (3) acceleration of droplet desolvation. Because droplets of small size mostly undergo acceleration instead of breakup by the high-speed nebulizer gas, the influence of the gas flow on the droplets is negligible in this work. When droplets are immersed in a high-speed gas flow, they will be accelerated. The

terminal velocity of a droplet depends on the relaxation time τ as defined in Equation (1):^[36]

$$\tau = \frac{p_d d^2 C_c}{18\eta} \quad (1)$$

where d and p_d are the diameter and density of the droplet, η is the coefficient of dynamic viscosity, and C_c is the Cunningham correction factor. Equation (1) shows that a smaller droplet with less relaxation time will reach the gas velocity more rapidly, thanks to the acceleration of the gas flow. In other words, smaller droplets would have a reduced flight time from the emitter of the capillary to the substrate. In addition, when the nebulizer gas meets droplets in the spray, the gas flow can remove evaporated solvent from the surface of the droplet, thereby boosting evaporation. Thus, smaller droplets are produced at higher gas flow rates.

These two factors have opposite effects on desolvation efficiency. In brief, higher gas flows increased evaporation rates and reduced evaporation times. When the flow rate was increased from 40 mL min⁻¹ to 60 mL min⁻¹, increasing evaporation produced smaller droplets and higher ion concentrations, resulting in smaller and more regular crystals. When the flow rate was increased from 60–100 mL min⁻¹, smaller crystals were again produced; however, there was not enough time to make the NaCl crystals grow with regular shapes. All these results are presented in Figure 5.

Conclusions

In this study, NaCl nanocrystals with cubic shapes were successfully produced from ultra-dilute NaCl solution (1 $\mu\text{g mL}^{-1}$) by electrospray crystallization. The morphologies of the nanoparticles were dependent on experimental variables that control the charge and the extent of desolvation. Static charge and solvent evaporation rate are crucial factors for crystal growth. Increasing charge and evaporation rate from the droplets would increase solution ionic strength and concentration and decrease the droplet size. These adjustments had a positive effect on crystal nucleation and growth, which resulted in smaller and more regular cubic-shaped crystals being generated. However, if the solution evaporated too rapidly, there was not enough time for the crystals to produce a regular morphology. These crucial factors can be controlled facilely by adjusting the ES parameters. In this work, we obtained cubic-shaped nanocrystals with a size of 32 nm. With appropriate parameters, we may obtain smaller NaCl nanocrystals with regular cubic shapes. Moreover, this technology is a green method, with nanoparticles being prepared without any stabilizers from aggregation. This study paves a way for crystallization of pharmaceuticals, proteins, optical materials, etc. ES technology is thus a promising candidate method for developing crystallization technologies.

Experimental Section

Materials: NaCl (AR grade) was obtained from Sinopharm Chemical Reagent Co., Ltd.; aqueous NaCl solution (1 $\mu\text{g mL}^{-1}$) was prepared

with Wahaha purified water for the electrospray crystallization process.

Electrospray Crystallization Setup: The electrospray crystallization setup shown in Scheme 1 with homemade electrospray nozzle and three-dimensional platform for fine-tuning was supported by Jiangxi Key Laboratory for Mass Spectrometry and Instrumentation, East China University of Technology. It mainly consists of a sample injection system (peristaltic pump donated by Kent Scientific Corporation, USA, and microsyringe supplied by Hamilton, USA), a high-voltage system (high-voltage source purchased from Boher High Voltage Power Supplies Co., Ltd, China), and a reaction system (plate heater purchased from Chemat Technology Co., Inc., USA, and silicon wafer for collecting obtained products purchased from Hefei Kejing Materials Technology Co., Ltd., China). The sample injection system is used to control the volume and flux speed of the solution during the injection process. A high voltage was applied to a microsyringe and the earthed line was also connected to a silicon wafer, which was placed on top of the plate heater for collection of samples. Nitrogen gas between quartz capillary and spray nozzle was applied to produce smaller droplets and to increase the solvent evaporation rate during the flight process.

Preparation of Crystals: All samples for characterization were prepared from extremely dilute NaCl solution (1 $\mu\text{g mL}^{-1}$) with spraying through a capillary and collection on the silicon wafer as collector (see Scheme 1). The inner diameter of the capillary was 0.1 mm, and high voltage was applied. The substrate temperature was set at 150 °C, and the solution throughput was fixed at 25 μL . Other parameters such as flight distance (distance from nozzle to the collector), solution flow rate, nebulizer gas flow rate, and voltage were set as follows.

Capillary Voltage: The capillary voltage was set at 0, +4, +8, and +12 kV, with a solution flow rate of 10 $\mu\text{L min}^{-1}$, a nebulizer gas of 60 mL min⁻¹, and a flight distance of 50 mm.

Solution Flow Rate: The parameters were set to different liquid flow rates of 10, 50, 100, and 200 $\mu\text{L min}^{-1}$, with a capillary voltage of +12 kV, a nebulizer gas of 60 mL min⁻¹, and a flight distance of 50 mm.

Distance from Nozzle to the Substrate: The parameters were set to different flight distances of 20, 30, 50, and 85 mm, with a capillary voltage of +12 kV, a nebulizer gas of 60 mL min⁻¹, and a solution flow rate of 10 $\mu\text{L min}^{-1}$.

Nebulizer Gas Flow Rate: The parameters were set to different nebulizer gas flow rates of 40, 60, 80, and 100 mL min⁻¹, with a capillary voltage of +12 kV, a flight distance of 50 mm, and a solution flow rate of 10 $\mu\text{L min}^{-1}$.

Characterization and Measurement: SEM and EDX were performed to investigate the morphologies, sizes, and component elements of nanocrystals with a FIB-SEM instrument (Helios Nanolab 600i from FEI Co.). The electron beam and working distance of the instrument were set to 10–20 kV and 4 mm, respectively.

X-ray diffraction (XRD) was carried out to determine the crystal structures with a Rigaku D/Max 2550 diffractometer with a graphite monochromator and use of Cu- K_{α} radiation ($\lambda = 1.5418 \text{ \AA}$), operating at 50 kV and 200 mA at room temperature. Data were obtained in the 2θ region between 10° and 70°; the scanning rate was 5° min⁻¹.

Acknowledgments

This work was supported by the National Natural Science Foundation of China (NSFC) (grant numbers 90922034, 21131002,

21427802, 21225522, and 21201075), the Program for Changjiang Scholars and Innovative Research Team in University (PCSIRT) (grant number IRT13054), and the Specialized Research Fund for the Doctoral Program of Higher Education (SRFDP grant 20110061130005).

Keywords: Crystal growth · Nanoparticles · Microreactors · Green chemistry

- [1] Z. Hu, C. Yan, P. Liu, Z. Huang, R. Ma, C. Zhang, R. Wang, Y. Zhang, F. Martinon, D. Miao, H. Deng, J. Wang, J. Chang, J. Chai, *Science* **2013**, *341*, 172–175.
- [2] X. Ma, X. Zhang, L. Yang, K. Wang, K. Jiang, Z. Wei, Y. Guo, *CrystEngComm* **2014**, *16*, 7933–7941.
- [3] R. J. Davey, S. L. Schroeder, J. H. ter Horst, *Angew. Chem. Int. Ed.* **2013**, *52*, 2166–2179; *Angew. Chem.* **2013**, *125*, 2220.
- [4] J. Puigmarti-Luis, *Chem. Soc. Rev.* **2014**, *43*, 2253–2271.
- [5] J.-T. Wang, J. Wang, J.-J. Han, *Small* **2011**, *7*, 1728–1754.
- [6] A. I. Toldy, A. Z. M. Badruddoza, L. Zheng, T. A. Hatton, R. Gunawan, R. Rajagopalan, S. A. Khan, *Cryst. Growth Des.* **2012**, *12*, 3977–3982.
- [7] D. S. Khvostichenko, J. M. Schieferstein, A. S. Pawate, P. D. Laible, P. J. A. Kenis, *Cryst. Growth Des.* **2014**, *14*, 4886–4890.
- [8] B. Zheng, J. D. Tice, L. S. Roach, R. F. Ismagilov, *Angew. Chem. Int. Ed.* **2004**, *43*, 2508–2511; *Angew. Chem.* **2004**, *116*, 2562.
- [9] X. X. Zhu, Q. H. Zhang, Y. G. Li, H. Z. Wang, *J. Mater. Chem. A* **2013**, *1*, 15559–15559.
- [10] J. Fang, C. W. Evans, G. J. Willis, D. Sherwood, Y. Guo, G. Lu, C. L. Raston, K. S. Iyer, *Lab Chip* **2010**, *10*, 2579–2582.
- [11] J. B. Fenn, M. Mann, C. K. Meng, S. F. Wong, C. M. Whitehouse, *Science* **1989**, *246*, 64–71.
- [12] A. Li, Q. Luo, S.-J. Park, R. G. Cooks, *Angew. Chem. Int. Ed.* **2014**, *53*, 3147–3150; *Angew. Chem.* **2014**, *126*, 3211.
- [13] R. King, R. Bonfiglio, C. Fernandez-Metzler, C. Miller-Stein, T. Olah, *J. Am. Soc. Mass Spectrom.* **2000**, *11*, 942–950.
- [14] V. V. Tolstikov, O. Fiehn, *Anal. Biochem.* **2002**, *301*, 298–307.
- [15] P. Kebarle, L. Tang, *Anal. Chem.* **1993**, *65*, 972A–986A.
- [16] G. M. H. Meesters, P. H. W. Vercoulen, J. C. M. Marijnissen, B. Scarlett, *J. Aerosol Sci.* **1990**, *21*, Supplement 1, S669–S672.
- [17] J. Xie, J. Jiang, P. Davoodi, M. P. Srinivasan, C.-H. Wang, *Chem. Eng. Sci.* **2015**, *125*, 32–57.
- [18] D. Duft, T. Achtzehn, R. Muller, B. A. Huber, T. Leisner, *Nature* **2003**, *421*, 128–128.
- [19] E. Ahadi, L. Konermann, *J. Am. Chem. Soc.* **2011**, *133*, 9354–9363.
- [20] N. Radacsi, R. Ambrus, T. Szunyogh, P. Szabo-Revesz, A. Stankiewicz, A. van der Heijden, J. H. ter Horst, *Cryst. Growth Des.* **2012**, *12*, 3514–3520.
- [21] L. Konermann, R. G. McAllister, H. Metwally, *J. Phys. Chem. B* **2014**, *118*, 12025–12033.
- [22] N. Radacsi, A. I. Stankiewicz, Y. L. M. Creighton, A. van der Heijden, J. H. ter Horst, *Chem. Eng. Technol.* **2011**, *34*, 624–630.
- [23] I. W. Lenggono, K. Okuyama, J. F. de la Mora, N. Tohge, *J. Aerosol Sci.* **2000**, *31*, 121–136.
- [24] D. Sarkar, M. K. Mahitha, A. Som, A. Li, M. Wlekinski, R. G. Cooks, T. Pradeep, *Adv. Mater.* **2016**, *28*, 2223–2228.
- [25] Z. Wang, S. M. King, E. Freney, T. Rosenoern, M. L. Smith, Q. Chen, M. Kuwata, E. R. Lewis, U. Poeschl, W. Wang, P. R. Buseck, S. T. Martin, *Aerosol Sci. Technol.* **2010**, *44*, 939–953.
- [26] T. M. Chen, H. M. Chein, *Aerosol Air Qual. Res.* **2006**, *6*, 305–321.
- [27] G. Biskos, A. Malinowski, L. M. Russell, P. R. Buseck, S. T. Martin, *Aerosol Sci. Technol.* **2006**, *40*, 97–106.
- [28] A. Tagantsev, C. Pawlaczyk, K. Brooks, N. Setter, *Integr. Ferroelectr.* **1994**, *4*, 1–12.
- [29] R. Ambrus, N. Radacsi, T. Szunyogh, A. van der Heijden, J. H. ter Horst, P. Szabo-Revesz, *J. Pharm. Biomed. Anal.* **2013**, *76*, 1–7.
- [30] A. F. Mejia, P. He, D. W. Luo, M. Marquez, Z. D. Cheng, *J. Colloid Interface Sci.* **2009**, *334*, 22–28.
- [31] A. Gomez, K. Tang, *Phys. Fluids* **1994**, *6*, 404–414.
- [32] A. Ganan-Calvo, J. Davila, A. Barrero, *J. Aerosol Sci.* **1997**, *28*, 249–275.
- [33] K. Altmann, R. D. Schulze, J. Friedrich, *Thin Solid Films* **2014**, *564*, 269–276.
- [34] R. M. Bain, C. J. Pulliam, R. G. Cooks, *Chem. Sci.* **2015**, *6*, 397–401.
- [35] R. Wang, P. Allmendinger, L. Zhu, A. J. Groehn, K. Wegner, V. Frankevich, R. Zenobi, *J. Am. Soc. Mass Spectrom.* **2011**, *22*, 1234–1241.
- [36] W. C. Hinds, *Aerosol technology: properties, behavior, and measurement of airborne particles*, John Wiley & Sons, California, **2012**.

Received: December 17, 2015

Published Online: March 24, 2016